NASA TECHNICAL NOTE

NASA TN D-4361

C.1

NASA TN D-4361

EFFECTS OF LEE-SURFACE VOLUME ADDITION ON LONGITUDINAL AERODYNAMICS OF A HIGH-LIFT-DRAG-RATIO WING-BODY CONFIGURATION AT MACH 6.0

by David R. Stone and George C. Ashby, Jr.

Langley Research Center
Langley Station, Hampton, Va.

NATIONAL AERONAUTICS AND SPACE ADMINISTRATION • WASHINGTON, D. C. • MARCH 1968

EFFECTS OF LEE-SURFACE VOLUME ADDITION ON LONGITUDINAL AERODYNAMICS OF A HIGH-LIFT-DRAG-RATIO WING-BODY CONFIGURATION AT MACH 6.0

By David R. Stone and George C. Ashby, Jr.

Langley Research Center
Langley Station, Hampton, Va.

NATIONAL AERONAUTICS AND SPACE ADMINISTRATION

For sale by the Clearinghouse for Federal Scientific and Technical Information
Springfield, Virginia 22151 – CFSTI price $3.00

EFFECTS OF LEE-SURFACE VOLUME ADDITION ON LONGITUDINAL AERODYNAMICS OF A HIGH-LIFT-DRAG-RATIO WING-BODY CONFIGURATION AT MACH 6.0

By David R. Stone and George C. Ashby, Jr.
Langley Research Center

SUMMARY

An aerodynamic investigation of the addition of volume to the leeward surface of a basic high-wing configuration has been made with volume additions varying from 9 percent to 92 percent of the basic wing-body volume. The free-stream Reynolds number based on body length was 9.5×10^6.

For a given volume addition, the experimental results show that span-height ratio, cross-sectional shape, and longitudinal contour had only secondary effects on the maximum lift-drag ratio. Calculations using shock theory indicate the effects of these parameters are overshadowed by the interaction between the volume-addition shock and the wing-body shock. The results indicate that a practical design practice would be to place the forebody volume addition at the wing apex, and the amount of afterbody volume added would thus be limited by the center-of-gravity location and the associated pitch characteristics of the vehicle.

The variation of the maximum lift-drag ratio with the volume efficiency parameter was found to be consistent with that of other high-wing configurations where the basic-body volume was varied. For a constant afterbody length, the maximum lift-drag-ratio variation with volume addition was found to be correlated by the parameter comprised of the product of the forebody slope and the percent volume added.

INTRODUCTION

The inherent slenderness of high-lift-drag-ratio (L/D) configurations generally poses problems in obtaining volume and a volume distribution adequate for packaging and center-of-gravity requirements. Packaging studies, alluded to in reference 1, indicate that the limiting height of such vehicles may also restrict the forward position of a seated crew. Such considerations led to the present aerodynamic investigation of the addition of volume to the leeward surface of a basic high-wing configuration.

Hypersonic high-lift-drag-ratio configurations ($L/D \geqq 3$) are generally composed of wing-body combinations with the body either suspended below (flat top) or above the wing (flat bottom) (ref. 2). The superiority of flat-top configurations over flat-bottom configurations or vice versa has not been absolutely established; however, a flat-top configuration, because of its inherent lateral stability and the possible favorable interference effects of the body-flow field on the windward wing surface (ref. 3), was selected for this investigation. The volume additions were made to the leeward surface of the wing because shielding at angles of attack for maximum lift-drag ratio $(L/D)_{max}$ should reduce the aerodynamic penalty. Since volume additions could be shaped either to provide head room for the crew, or to fit the general contour of a variety of other equipment, the effect of cross-sectional shape was also investigated. Some investigations (for example, ref. 4) have shown the effect of adding volume on the lee side of a wing which is on top of a half body; however, the size and shape of the added volume was the same as that of the body underneath and no systematic variation of the added volumes was made. In the present parametric aerodynamic study, volume additions varying from 9 percent to 92 percent of the basic wing-body volume were made. The experimental results were obtained in the Langley 20-inch Mach 6 tunnel at a free-stream Reynolds number based on body length of 9.5×10^6. Some of the results of this investigation are presented in reference 5.

SYMBOLS

b	maximum width of volume addition, centimeters
ΔC_A	incremental axial-force coefficient, $\frac{\text{Axial force}}{q_\infty S}$
C_D	drag coefficient, $\frac{\text{Drag}}{q_\infty S}$
C_L	lift coefficient, $\frac{\text{Lift}}{q_\infty S}$
C_m	pitching-moment coefficient, $\frac{\text{Pitching moment}}{q_\infty S \mathscr{l}}$
$C_{m,o}$	pitching-moment coefficient at $\alpha = 0^o$
ΔC_N	incremental normal-force coefficient, $\frac{\text{Normal force}}{q_\infty S}$
h	maximum height of volume addition, centimeters
$\mathscr{l}$	total length of vehicle, centimeters

l_b	length of afterbody of volume addition, centimeters
l_n	length of forebody of volume addition, centimeters
L/D	lift-drag ratio
$(L/D)_{max}$	maximum value of lift-drag ratio
q_∞	free-stream dynamic pressure, newtons/meter^2
R_∞	Reynolds number based on free-stream conditions and model length
S	planform area of wing, centimeters^2
V	total volume, centimeters^3
V_o	volume of basic configurations including wings, centimeters^3
ΔV	volume of the addition, centimeters^3
$\frac{\Delta V}{V_o}$	increase in volume, percent
x_{cp}	center of pressure from leading edge, percent
α	angle of attack, degrees
θ	forebody slope, degrees or radians

APPARATUS, TESTS, AND ACCURACY

The investigation was conducted in the Langley 20-inch Mach 6 tunnel. The tunnel is a blowdown atmospheric type which has been described in reference 6. The tests were conducted at a nominal Mach number of 6.00, a stagnation pressure of 27.2 atmospheres $\left(2.76 \times 10^6 \frac{N}{m^2}\right)$, and a stagnation temperature of 477° K. The free-stream Reynolds number based on model length was 9.5×10^6. The location of boundary-layer transition was not experimentally determined for these configurations. However, transition studies on somewhat similar wings under the same tunnel conditions suggest that at zero angle of attack, transition would start on the center line of the upper surface of the basic configuration before the 30-percent station.

Forces and moments on the configurations were measured by an internally mounted water-cooled six-component strain-gage balance. Base-pressure measurements were made and the measured axial force was corrected to a condition of free-stream base pressure. The model angle of attack was set by reflecting a light beam for a prism located in the surface of the model onto a precalibrated screen, as described in reference 7. This method of measuring angle of attack is estimated to be accurate to $\pm 0.10^{\circ}$. The Mach number was measured for each test point to an accuracy of ±0.01 by use of a total-pressure probe.

On the basis of the balance calibration, readout accuracy, and dynamic-pressure accuracy, it is estimated by the method of least squares that the aerodynamic coefficients are accurate within the following maximum average limits:

C_D	±0.0005
C_L	±0.0020
C_m	±0.0002
L/D	±0.2000

MODELS

The basic wing-body combination used in this investigation consisted of a body having the same length and volume as the minimum-drag body for fixed length and volume derived by Miele in reference 8 and a wing contoured to the body shock shape at a Mach number of 19. The basic body had a 2:1 half-elliptical cross section and the same cross-sectional area distribution as a body of revolution with a fineness ratio of 7.5. This basic shape had previously been studied in performance investigations in the Langley 22-inch helium tunnel and appeared to be favorable as a possible entry vehicle shape, as indicated in reference 9.

The coordinates for the wing and body are given in figure 1. The basic wing-body combination is shown in figure 2, a typical volume addition being located on the upper surface of the wing. The volume additions were divided into four groups as shown in figures 3 and 4 and in table I. Group A volume additions consisted of a half-quadrangular regular-pyramid forebody followed by a rectangular-parallelpiped afterbody with a l_b/l ratio of 0.30. For a given volume, this group had two different values of b/h and a total length of 38.10 cm. Group B volume additions consisted of a half-circular cone forebody followed by a half-circular cylinder afterbody with an l_b/l ratio of 0.30 and a total length of 38.10 cm. Group C volume additions had the same afterbody lengths as groups A and B; however, their forebodies were approximately half as long and therefore were labeled short-forebody volume additions. These bodies had rectangular cross sections and a total length of 25.01 cm. Group D volume additions have both rectangular and semicircular cross sections and approximately the same forebody length as group C,

but their l_b/l ratio was extended to 0.66. This group had a total length of 38.10 cm. The minimum-drag volume addition (fig. 3(b)) had the same area distribution as the original 2:1 half-ellipse body, but had a semicircular cross section.

RESULTS AND DISCUSSION

Effect of Volume Addition on Longitudinal-Force Components

Experimental data.- Figure 5 presents the measured longitudinal-force coefficients for the various volume additions. In general, the curves follow trends consistent with what would be expected from a simple physical analysis; that is, because the volume added on top should increase the axial force and decrease the normal force of the total configuration, it would be expected that the volume addition to the lee side would result in a decrease of $(L/D)_{max}$. In addition, the forces contributed by the volume addition on the leeward side should decrease as shielding increases; therefore, to benefit from the shielding the α for $(L/D)_{max}$ would be expected to increase. Figure 5, however, shows that the magnitude of $(L/D)_{max}$ did not always vary directly with the amount of volume added. For example, in figure 5(a), volume additions A-5 and A-6 have the same value of $(L/D)_{max}$ and α for $(L/D)_{max}$, but, their volumes are different (46 percent and 69 percent, respectively). Table I shows that volume addition A-5 is still exposed at the α for $(L/D)_{max}$ whereas volume addition A-6 is not. Several other volume additions are also exposed at α for $(L/D)_{max}$. (See table I.) However, the effect on their force coefficients of being exposed as compared with those not exposed is not obvious from the plots of figure 5.

The volume addition of groups A and B all have the same drag coefficient beyond $\alpha = 8^{\circ}$, whereas the lift coefficients are different. To determine why the volume additions had these observed effects on the force coefficients and $(L/D)_{max}$, some basic aerodynamic relations were examined. Theoretically, $(L/D)_{max}$ occurs at the angle of attack where $dC_L/dC_D = C_L/C_D$. This relationship can be represented on a plot of the variation of C_L with C_D by a line drawn from the origin tangent to the curve. (See fig. 6.) The addition of volume to the basic vehicle alters the curve of C_L plotted against C_D, and the manner in which the curve is altered governs the effect of the volume addition on $(L/D)_{max}$ and the α for $(L/D)_{max}$.

In the present investigation where volume was added to the leeward side, the normal-force increment ΔC_N due to the addition should be negative and the axial-force increment ΔC_A, positive. The magnitudes of both forces resulting from the added volumes should decrease with increasing α because of shielding effects. The signs of these forces coupled with their trigonometric relationships with ΔC_L and ΔC_D (that is, $\Delta C_L = \Delta C_N \cos \alpha - \Delta C_A \sin \alpha$; $\Delta C_D = \Delta C_N \sin \alpha + \Delta C_A \cos \alpha$) cause both

increments in ΔC_L to subtract from the total lift, whereas those in ΔC_D are of opposite signs. As a consequence, as α increases ΔC_D decreases relative to ΔC_L. The combined effect of the decrease in forces with α and the decrease of the magnitude of ΔC_D relative to that of ΔC_L can be considered as a shift and a counterclockwise rotation of the curve of C_L plotted against C_D so that the $(L/D)_{max}$ has a lower value and occurs at a higher α. These results can be observed in figure 6. This figure presents the drag polars for the volume additions of group B, which are typical for all of the volume additions. Note the decrease in drag at $\alpha \geqq 6^o$ for some volume additions.

Calculation of incremental forces due to volume addition.- To check the usefulness of theory for predicting the effect of volume addition on the $(L/D)_{max}$ of the basic vehicle, the normal- and axial-force increments due to several of the volume additions were calculated. Since all the forebodies of the additions have conical profiles, the pressures were calculated primarily by the use of conical-flow theory.

The pressures on the top surface of the pyramid forebody which originated at the wing apex were calculated by using free-stream flow conditions and shock theory until the angle of attack became greater than the forebody slope. Beyond that angle of attack, the surface pressures were obtained by expanding the free-stream flow to the angle of the surface with Prandtl-Meyer relations. For the side surfaces of the forebodies, the pressures were computed by using shock theory; however, the upstream-flow properties were assumed to be equal to those for the lee surface of the wing which were calculated by using Prandtl-Meyer expansions. The pressure on the wing surface between the side surfaces of the volume addition and the shock generated by the volume addition was assumed to be the average of the pressure on the side surface and that calculated immediately behind the conical shock. (See ref. 3.) In one case, the calculations for the flat surfaces of a pyramidal body were also made with the use of two-dimensional oblique-shock theory. For this calculation the pressure on the wing surface between the side surfaces of the volume addition and the shock generated by the volume addition was assumed to be the same as that on the side surface. The expansions at the junction of the forebodies and afterbodies of the volume additions were also considered in the calculations.

Figure 7 presents the comparison between the calculated and measured increments in normal force and axial force for several of the volume additions of group A. Although the calculations using conical-flow theory would have been somewhat more appropriate for group B, the difference between theory and experiment for group A is typical for all groups and is presented to show the oblique-shock theory. The calculated values follow, in general, the trend of the measured values with angle of attack; however, the calculated and measured values do not agree. The calculated values of ΔC_A do not contain any skin-friction estimates; however, it is believed that these values are small and would

not significantly alter the results. Both the conical- and oblique-shock theories underpredict the axial-force increments, but the conical-shock theory underpredicts and the oblique-shock theory overpredicts the normal force. The underprediction was somewhat surprising, especially with respect to the axial-force increment, since for that component only the frontal area of the forebody addition was thought to be involved. It was noted from the calculations, that the shock resulting from the side surface of even the smallest forebody of the tests extends to or beyond the leading edge of the wing (for both the conical- and oblique-shock theories). The interaction between it and the wing leading-edge shock evidently alters the pressure field about the wing-body configuration and around the volume addition so that the contributions of each to the normal and axial forces is considerably different than each would be alone.

Parametric Effects on $(L/D)_{max}$

Figure 8 shows the variation of $(L/D)_{max}$ with the volume parameter $V^{2/3}/S$ for all the present configurations that can be compared with the data from reference 2. This reference shows the trend for a half-cone—delta-wing configuration at a Reynolds number of 1.5×10^6 and a Mach number M of 6.8. The present data are noted to follow the general trend of the simple cone—delta-wing configuration with respect to the volume parameter; however, the width of the data band indicates that the shape of the added volume can be changed to reduce the penalty on $(L/D)_{max}$.

The present data are also plotted in figure 9 against percent volume added, the percentage loss in $(L/D)_{max}$ being shown on the right. The loss in $(L/D)_{max}$ with volume increase reaches a value of 36 percent for the 92-percent volume addition that extends to the wing apex. For a constant volume and afterbody-length, shortening the forebody significantly increased the loss in $(L/D)_{max}$, especially at higher volumes. The arrow within the data bands in figure 9 shows the effect of increasing span-height ratio (b/h).

This b/h effect is examined more closely in figure 10. It is recalled that the theoretical calculations revealed that the shock generated by the side of the forebody of the smallest volume addition of the tests extends to the wing leading edge. Increases in b/h result in increases in shock angle of the side of the forebody which may change the interference effect between it and the wing leading-edge shock. Therefore, the effect of increasing b/h for the isolated volume addition might be overshadowed by the shock interference effects. Although the benefit to $(L/D)_{max}$ of increasing b/h is indicated to be only slight, there would probably be a benefit in reduced heat protection if b/h were increased so that the upper surface of the volume would never be exposed at α for $(L/D)_{max}$.

The limited data indicate little dependence on cross-sectional shape since the semicircular cross-sectional data are in good agreement with the rectangular cross-sectional data at the same values of b/h and l_b/l. The effect of adding volume by means of a minimum-drag body with a semicircular cross section was also studied. This addition had the same volume as the body under the wing and increased the total volume including the wing by 91 percent. The data point for this body, which is plotted in both figures 9 and 10, shows that very little benefit would be realized by its use, at least for the larger volume additions. This result, along with the insensitivity of cross-sectional shape, indicates that the contour shape of the added volume can be dictated by other considerations, such as aerodynamic heating or packaging requirements.

In hypersonic flow, the value of L/D for a given cross-sectional body with a constant afterbody length is related to the forebody slope, as well as the volume. Therefore, a simple parameter $\theta \frac{\Delta V}{V_o}$ consisting of the forebody slope in radians and the percentage volume added was explored as a correlating parameter (fig. 11). This parameter gives good correlation of the data for both the semicircular and rectangular cross-sectional bodies and for both the long-forebody and short-forebody additions.

To investigate the effect of changing the location of the forebody apex relative to the wing apex, two of the short-forebody volume additions were moved to the wing's apex and the volume was increased by increasing the afterbody length. (See figs. 9 and 11.) The effect on $(L/D)_{max}$ is only slight for both volume additions. Other volume additions with an l_b/l ratio of 0.66 are shown in both figures 9 and 11. In figure 11, the values of $(L/D)_{max}$ for l_b/l of 0.66 lie along another curve. Since several of these values were obtained by moving the short forebody forward to the wing apex and adding volume behind it without much loss in $(L/D)_{max}$, it appears that the correlating curves are a family which depend on the afterbody length. Therefore, a practical design practice would be to place the forebody at the wing apex and add afterbody volume. The amount of afterbody volume added would be limited by the center-of-gravity location and associated pitch characteristics of the vehicle.

The effect on the pitch characteristic of adding volume to the top of the present vehicle is shown in figure 12 for volume groups A and B, which are typical. The $C_{m,o}$ and the trim angle of attack decrease as volume increases; thus, for the larger volume additions with a fixed center-of-gravity location, the vehicle trims closer to α for $(L/D)_{max}$.

CONCLUDING REMARKS

An aerodynamic investigation of the addition of volume to the leeward surface of a basic high-wing configuration has been made. Theoretical calculations using both

conical- and oblique-shock theories indicate the trends for the increments in normal-force and axial-force coefficients due to the volume addition, but the conical-shock theory underpredicts and the oblique-shock theory overpredicts the normal force. A comparison of calculations and experimental data indicate that a large portion of the effect of the volume addition on these parameters is a result of interaction between the leading-edge shock of the wing-body configuration and the forebody shock of the volume addition. Although the effect of an increase of volume on this interaction effect can be discerned by a change in lift-drag ratio, evidently, for a given volume addition, the interaction is so predominant it overshadows the parametric change. The experimental results show that variations in span-height ratio, cross-sectional shape, and longitudinal contour had only secondary effects on the maximum lift-drag ratio. The results also show that a practical design practice would be to place the forebody of the volume addition at the wing apex and add afterbody volume. The amount of volume added would be limited by the center-of-gravity location and the associated pitch characteristics of the vehicle. The variation of $(L/D)_{max}$ with the volume parameter $V^{2/3}/S$ was found to be consistent with that of other high-wing configurations where the basic-body volume was varied. In addition, the variation of maximum lift-drag ratio was found to be correlated by the simple parameter comprised of the product of the forebody slope and the percent volume added.

Langley Research Center,
National Aeronautics and Space Administration,
Langley Station, Hampton, Va., August 28, 1967,
124-07-02-57-23.

REFERENCES

1. Love, Eugene S.: Manned Lifting Entry. Astronaut. Aeron., vol. 4, no. 5, May 1966, pp. 54-64.

2. Fetterman, David E.; Henderson, Arthur, Jr.; Bertram, Mitchel H.; and Johnston, Patrick J.: Studies Relating to the Attainment of High Lift-Drag Ratios at Hypersonic Speeds. NASA TN D-2956, 1965.

3. Fetterman, David E.: Favorable Interference Effects on Maximum Lift-Drag Ratios of Half-Cone Delta-Wing Configurations at Mach 6.86. NASA TN D-2942, 1965.

4. Burchfield, C. G.: Force Tests of Several Sharp Leading Edge Wing-Body Combinations at Mach 8. AEDC TN-61-46, U.S. Air Force, May 1961.

5. Ashby, George C., Jr.; and Stone, David R.: Aerodynamic Effect of Volume Addition to a High L/D Wing/Body at Mach 6.0. J. Spacecraft Rockets, vol. 4, no. 2, Feb. 1967, pp. 277-279.

6. Sterrett, James R.; and Emery, James C.: Extension of Boundary-Layer-Separation Criteria to a Mach Number of 6.5 by Utilizing Flat Plates With Forward-Facing Steps. NASA TN D-618, 1960.

7. Ashby, George C., Jr.; and Fitzgerald, Paul E., Jr.: Longitudinal Stability and Control Characteristics of Missile Configurations Having Several Highly Swept Cruciform Fins and a Number of Trailing-Edge and Fin-Tip Controls at Mach Numbers From 2.21 to 6.01. NASA TM X-335, 1961.

8. Miele, Angelo: Optimum Slender Bodies of Revolution in Newtonian Flow. Tech. Rept. No. 56, Flight Sci. Lab., Boeing Sci. Res. Lab., Apr. 1962.

9. Woods, W. C.; Johnston, P. J.; Molloy, J. K.; and Henderson, A., Jr.: Recent Studies of Factors Affecting High Lift-Drag Ratios at $M = 19$ in Helium. AIAA Paper No. 67-138, Jan. 1967.

TABLE I.- IMPORTANT PARAMETERS FOR THE VOLUME ADDITIONS A TO D PLUS MINIMUM-DRAG BODY

Volume addition	b, cm	h, cm	l_n, cm	l_b, cm	l_b/l	$\frac{V^{2/3}}{S}$	b/h	$\frac{\Delta V}{V_o}$, percent	θ, deg	$\theta \frac{\Delta V}{V_o}$, radian-percent	α at $(L/D)_{max}$, deg
A-1	2.54	0.95	26.67	11.43	0.30	0.256	2.67	11.50	2.05	0.41	3.00
A-2	2.54	1.91	26.67	11.43	.30	.274	1.33	23.00	4.08	1.64	3.00
A-3	5.08	.95	26.67	11.43	.30	.274	5.35	23.00	2.05	.82	3.00
A-4	5.08	1.91	26.67	11.43	.30	.306	2.66	46.00	4.08	3.28	5.00
A-5	2.54	3.81	26.67	11.43	.30	.306	.67	46.00	8.13	6.53	6.00
A-6	6.25	2.29	26.67	11.43	.30	.337	2.73	69.00	4.90	5.90	6.00
A-7	7.62	2.54	26.67	11.43	.30	.367	3.00	92.00	5.45	8.75	7.00
A-8	5.08	3.81	26.67	11.43	.30	.367	1.33	92.00	8.13	13.05	7.00
A-9	3.81	3.81	26.67	11.43	.30	.337	1.00	69.00	8.13	9.79	6.00
B-1	7.02	3.51	26.67	11.43	.30	.367	2.00	92.00	7.35	11.80	8.00
B-2	5.60	2.80	26.67	11.43	.30	.324	2.00	58.80	6.03	6.19	6.00
B-3	4.96	2.48	26.67	11.43	.30	.306	2.00	46.00	5.33	4.28	6.00
B-4	3.52	1.76	26.67	11.43	.30	.273	2.00	23.00	3.10	1.24	4.00
C-1	2.54	.95	13.58	11.43	.30	.252	2.67	9.03	4.08	.64	3.00
C-2	2.54	1.91	13.58	11.43	.30	.266	1.33	18.00	8.00	2.51	5.00
C-3	5.08	.95	13.58	11.43	.30	.266	5.35	18.00	4.17	1.31	4.50
C-4	5.08	1.91	13.58	11.43	.30	.292	2.66	36.10	8.00	5.04	6.00
C-5	2.54	3.81	13.58	11.43	.30	.292	.67	36.10	15.68	9.88	6.00
C-6	5.08	3.81	13.58	11.43	.30	.342	1.33	72.20	15.68	19.76	8.00
D-1	4.94	2.47	13.08	25.02	.66	.334	2.00	66.50	10.71	12.43	6.00
D-2	3.50	1.75	13.08	25.02	.66	.288	2.00	33.20	7.61	4.41	4.50
D-3	2.54	1.91	13.08	25.02	.66	.288	1.33	33.20	8.30	4.81	5.50
D-4	2.54	3.81	13.08	25.02	.66	.334	.67	66.50	16.28	18.90	7.00
Minimum drag body	7.18	3.59	----	----	---	0.366	2.00	91.00	4.63	7.35	7.00

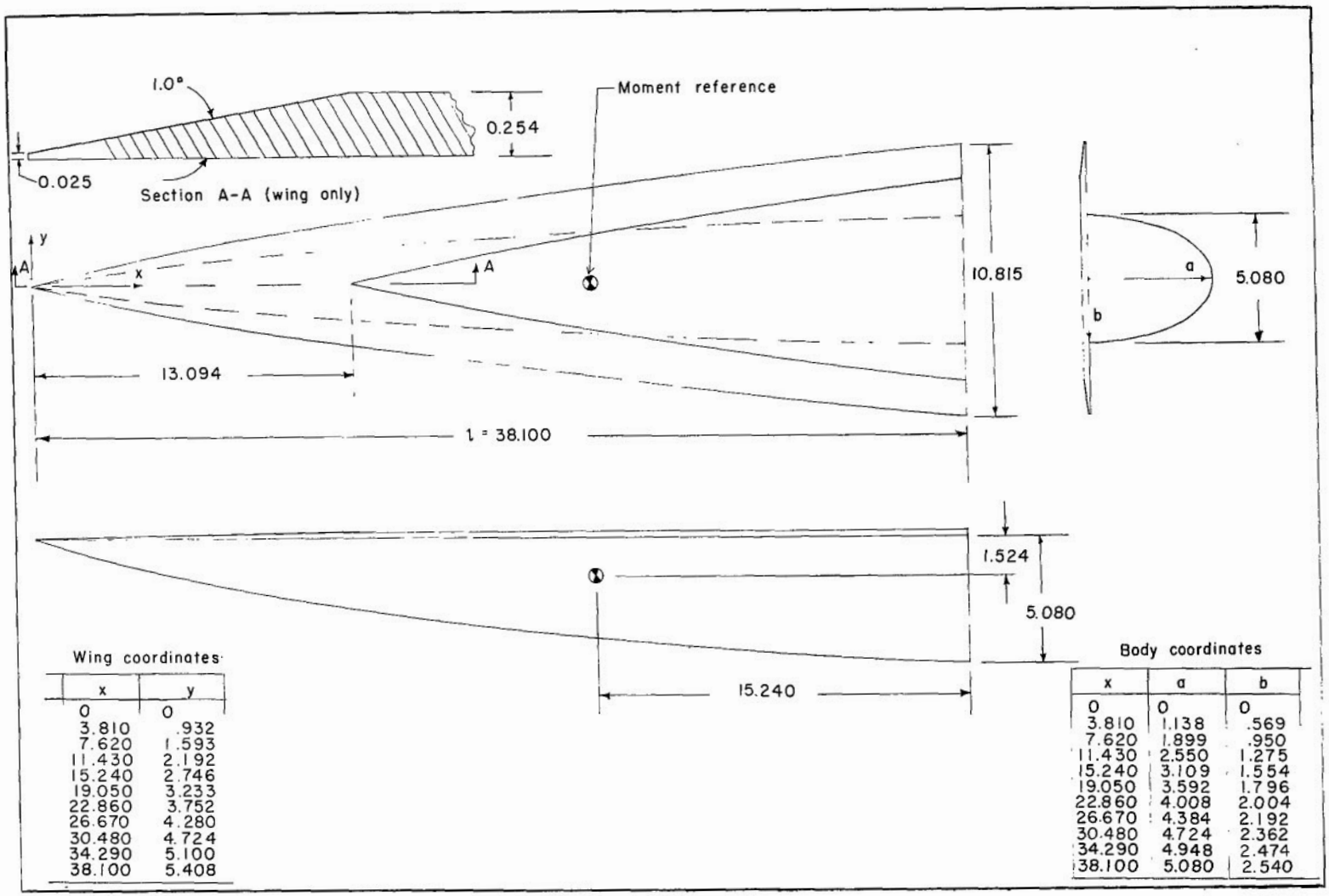

Wing coordinates

x	y
0	0
3.810	.932
7.620	1.593
11.430	2.192
15.240	2.746
19.050	3.233
22.860	3.752
26.670	4.280
30.480	4.724
34.290	5.100
38.100	5.408

Body coordinates

x	a	b
0	0	0
3.810	1.138	.569
7.620	1.899	.950
11.430	2.550	1.275
15.240	3.109	1.554
19.050	3.592	1.796
22.860	4.008	2.004
26.670	4.384	2.192
30.480	4.724	2.362
34.290	4.948	2.474
38.100	5.080	2.540

Figure 1.- Sketch of basic high-wing configuration. All dimensions are in centimeters.

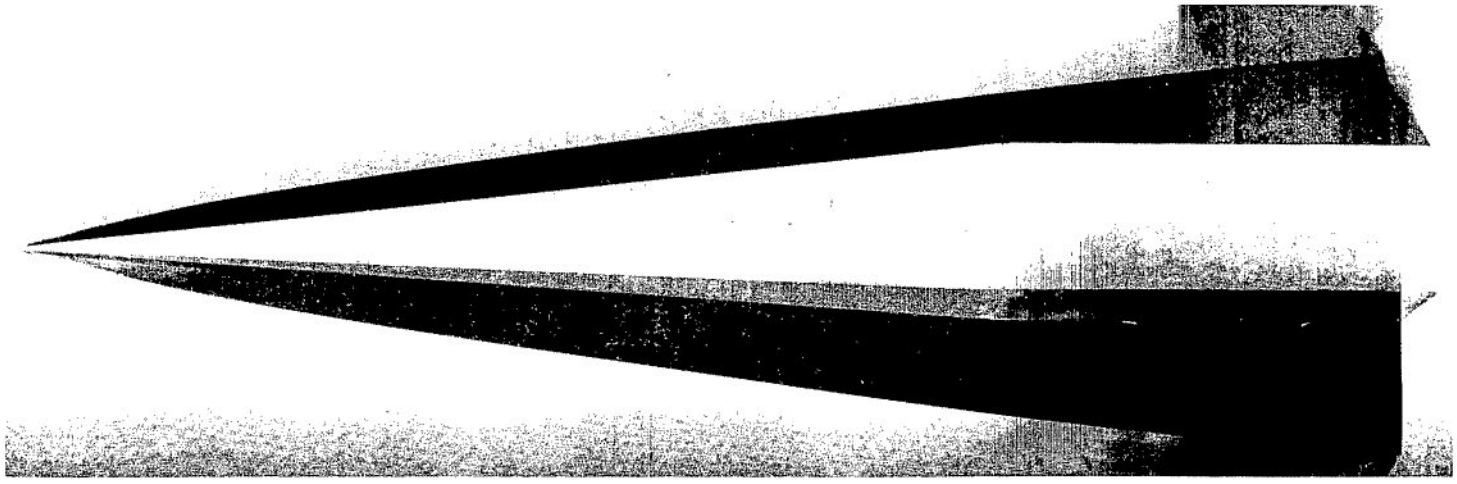

(a) Top view.

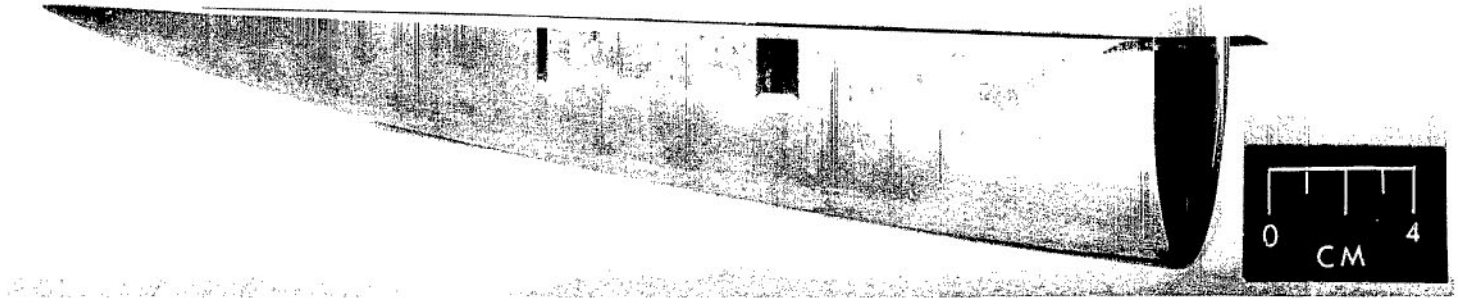

(b) Side view. L-67-6700

Figure 2.- Photograph of basic high-wing configuration with volume addition A-9.

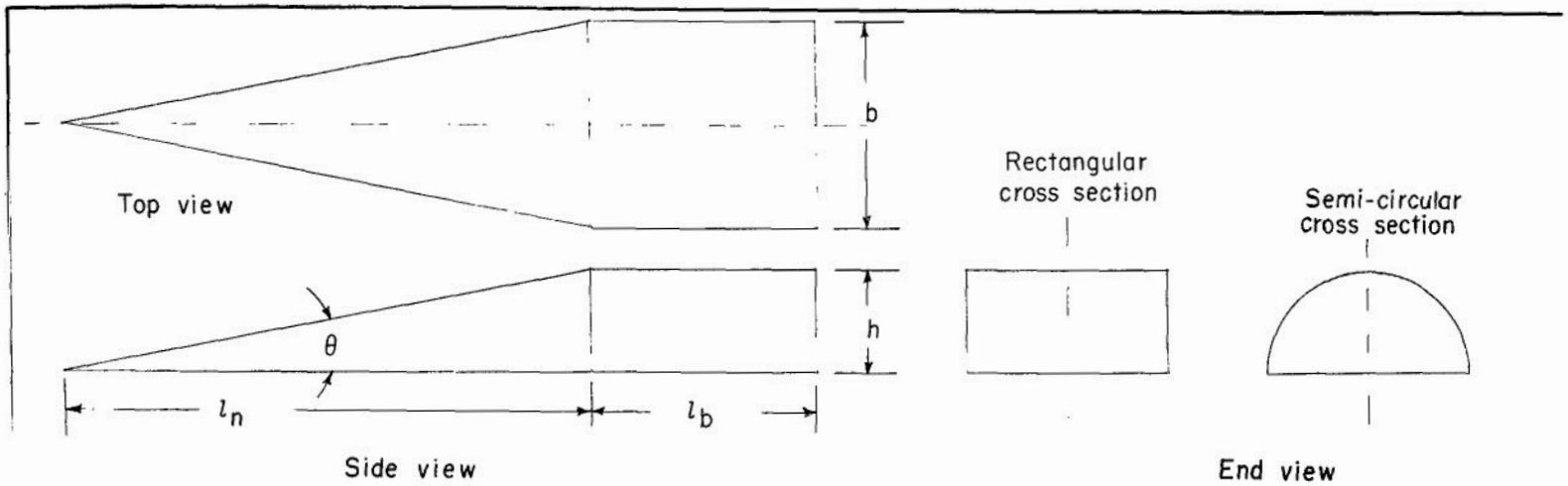

(a) Sketch of volume additions A to D.

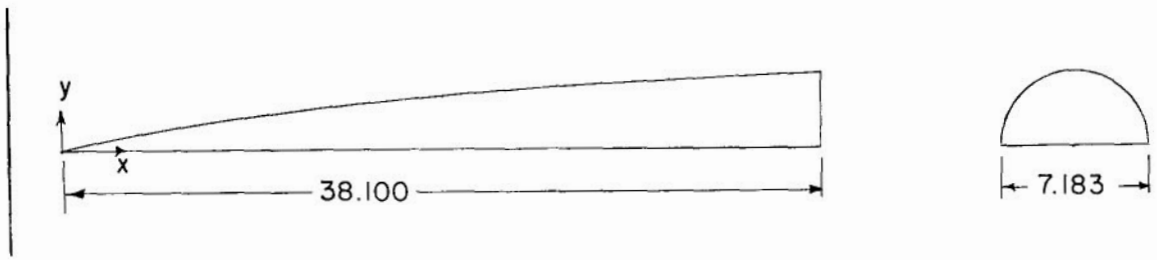

Minimum drag model coordinates

x	y
0	0
3.810	.805
7.620	1.344
11.430	1.803
15.240	2.197
19.050	2.540
22.860	2.835
26.670	3.099
30.480	3.340
34.290	3.498
38.100	3.592

(b) Sketch of minimum drag volume addition.

Figure 3.- Sketches of volume additions. All dimensions are in centimeters.

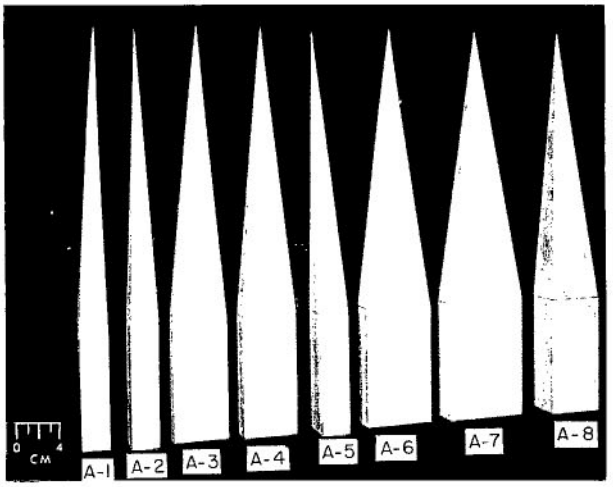

(a) Long forebody.

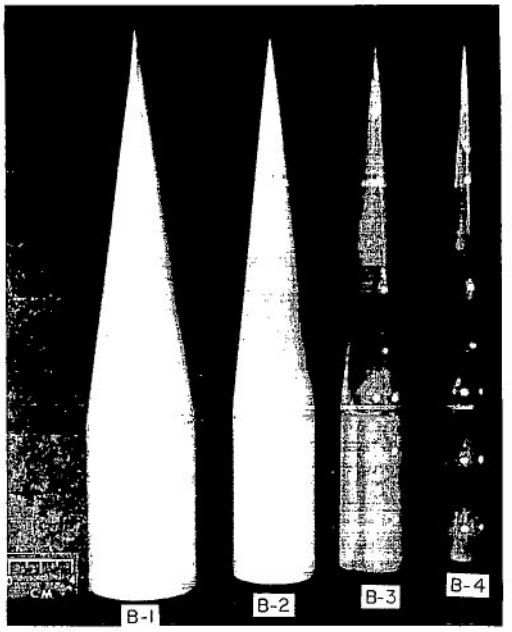

(b) Semicircular.

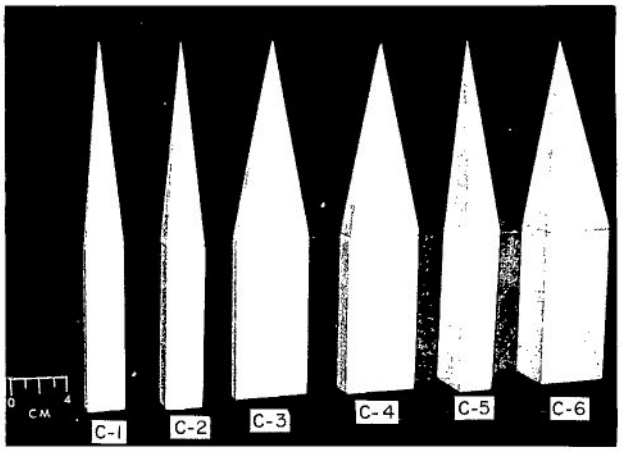

(c) Short forebody.

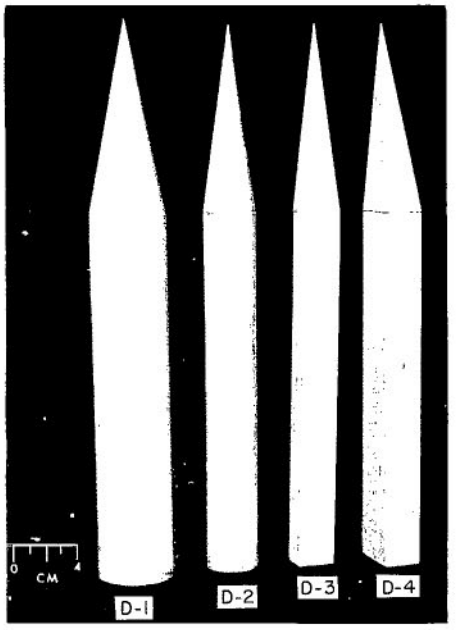

(d) l_b/l extended from 0.30 to 0.66.

Figure 4.- Photographs of volume additions. L-67-8701

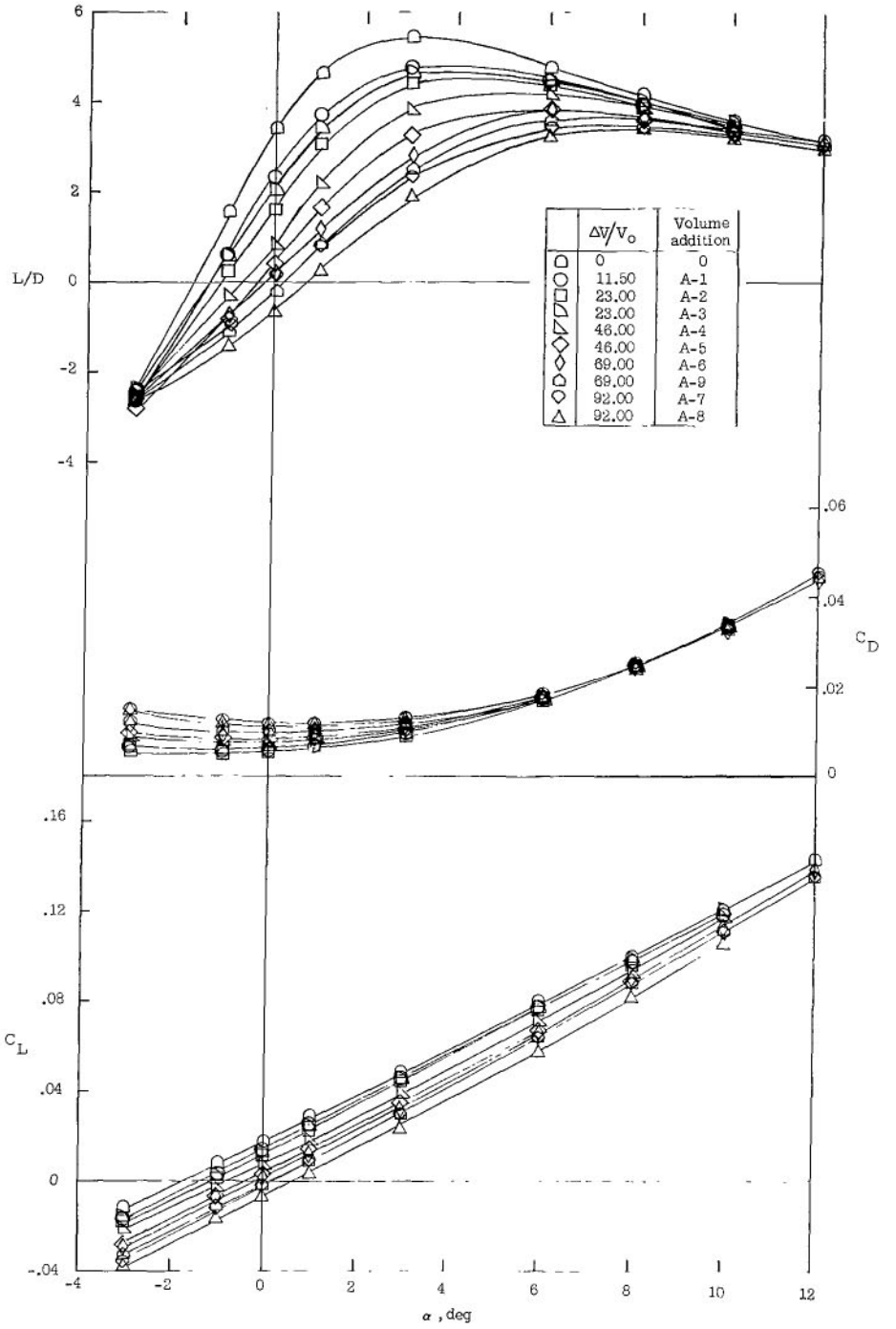

(a) Long forebody with square cross section. Group A.

Figure 5.- Measured longitudinal-force coefficients for the volume additions.

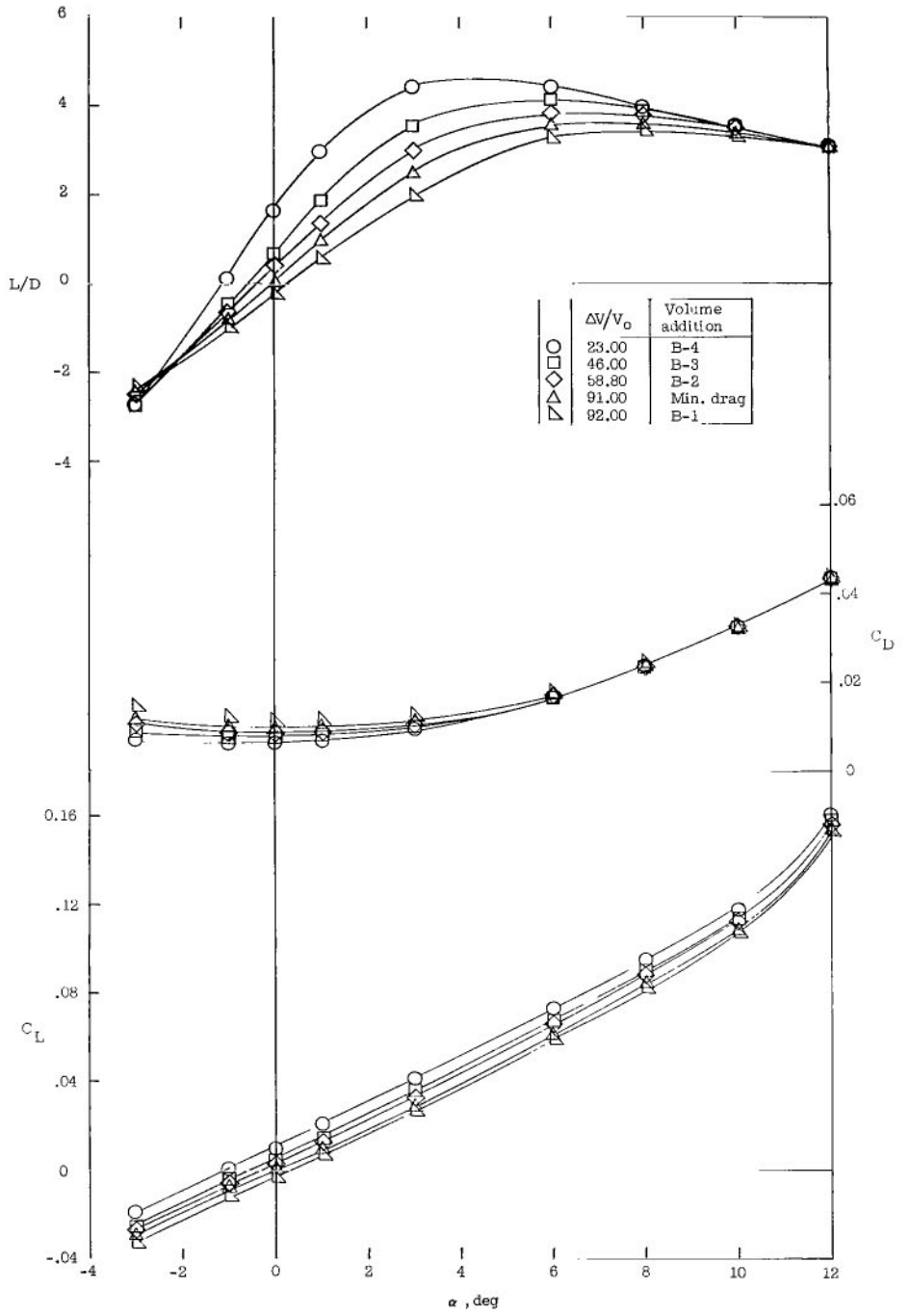

(b) Long forebody with semicircular cross section. Group B.

Figure 5.- Continued.

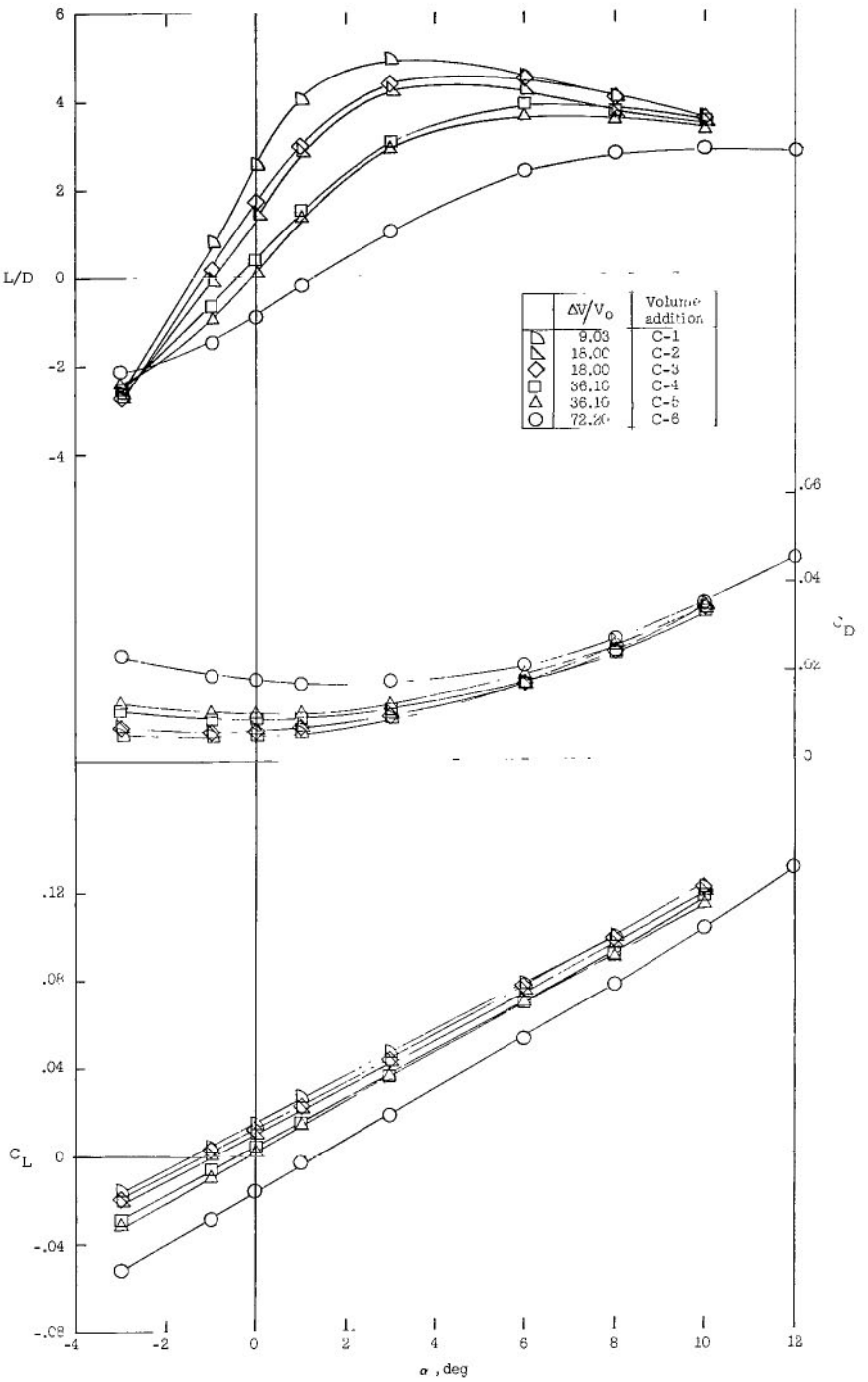

(c) Short forebody. Group C.

Figure 5.- Continued.

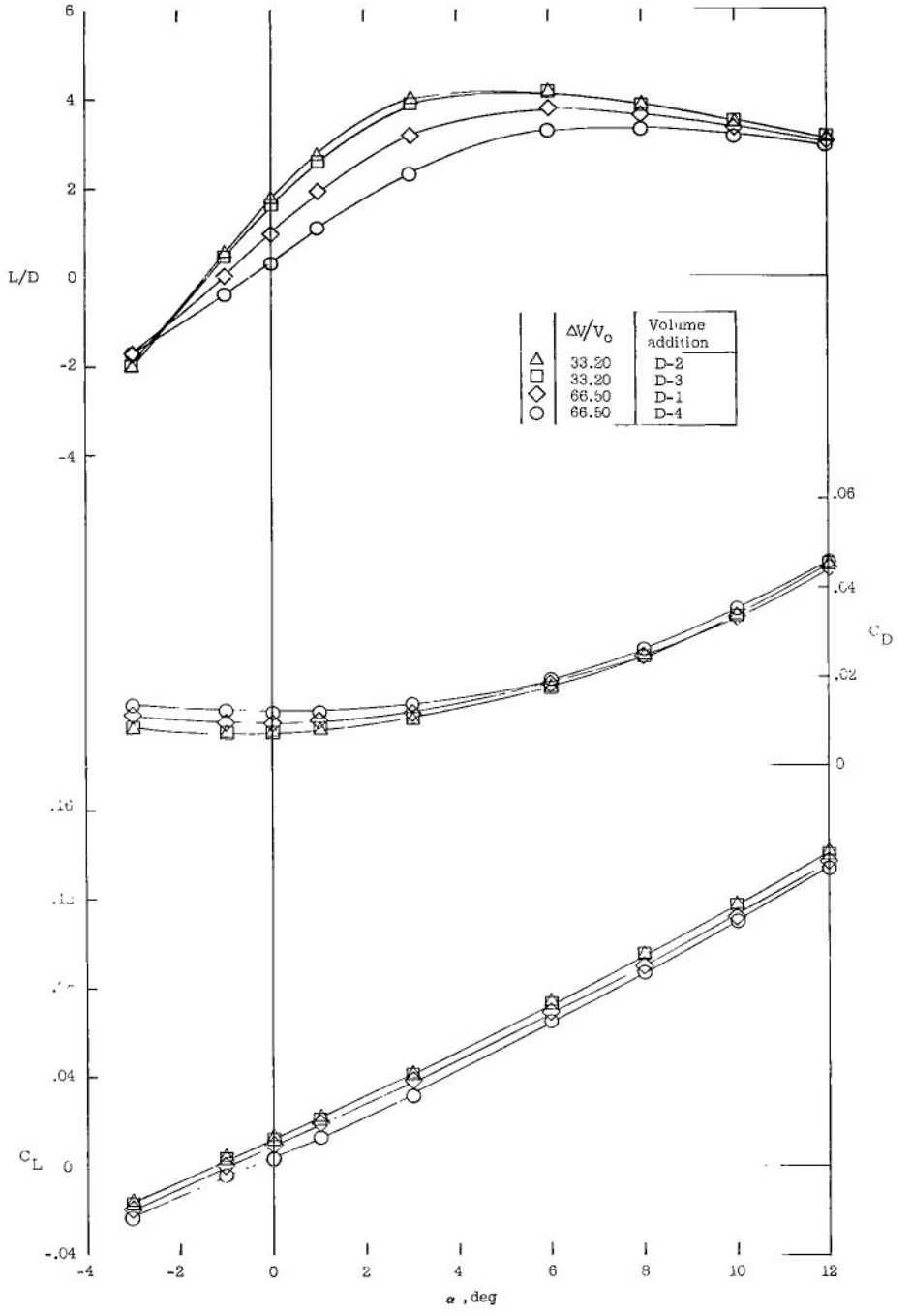

(d) l_b/l extended to 0.66. Group D.

Figure 5.- Concluded.

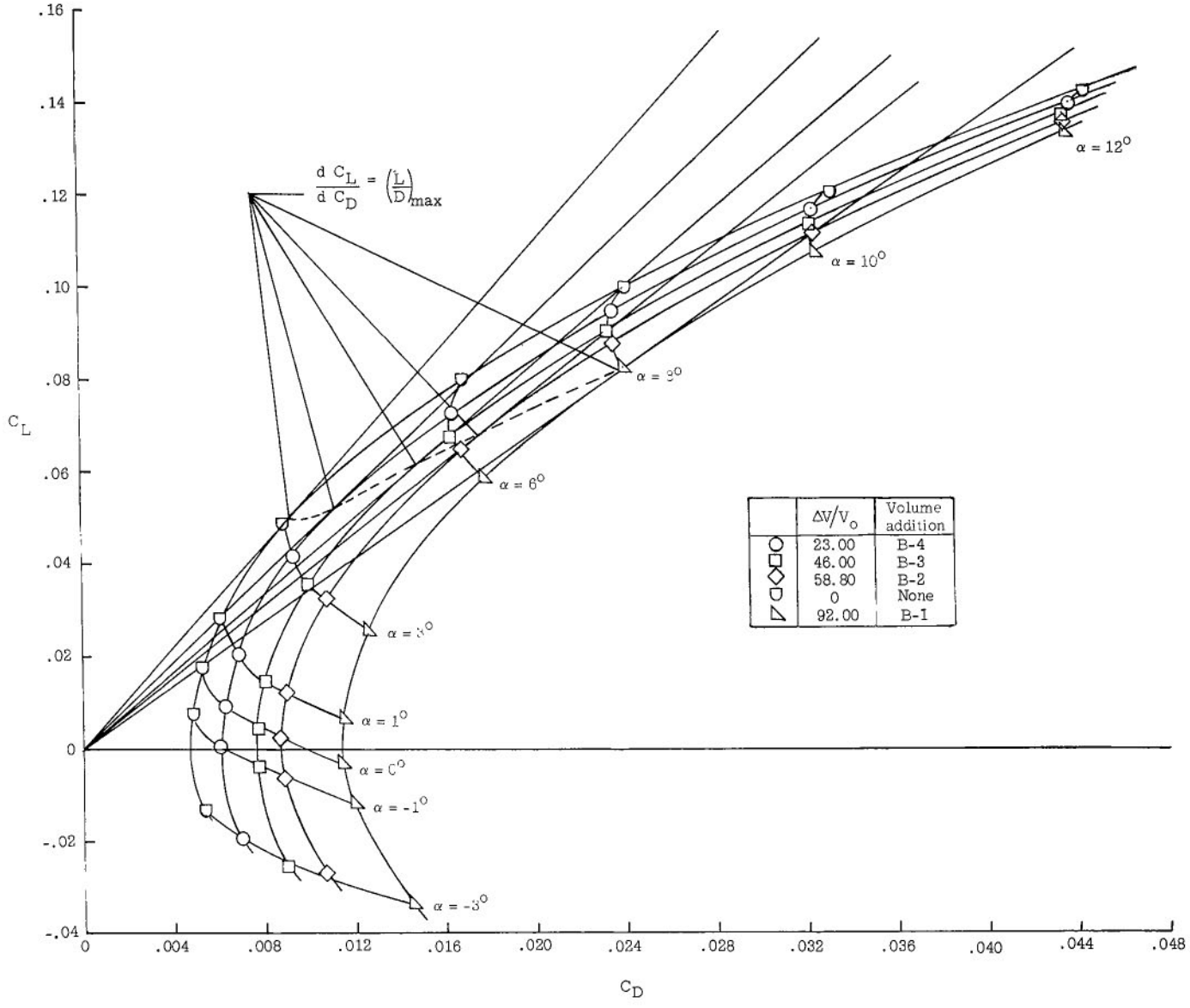

Figure 6.- Drag polars for the basic configurations without and with the volume additions of group B.

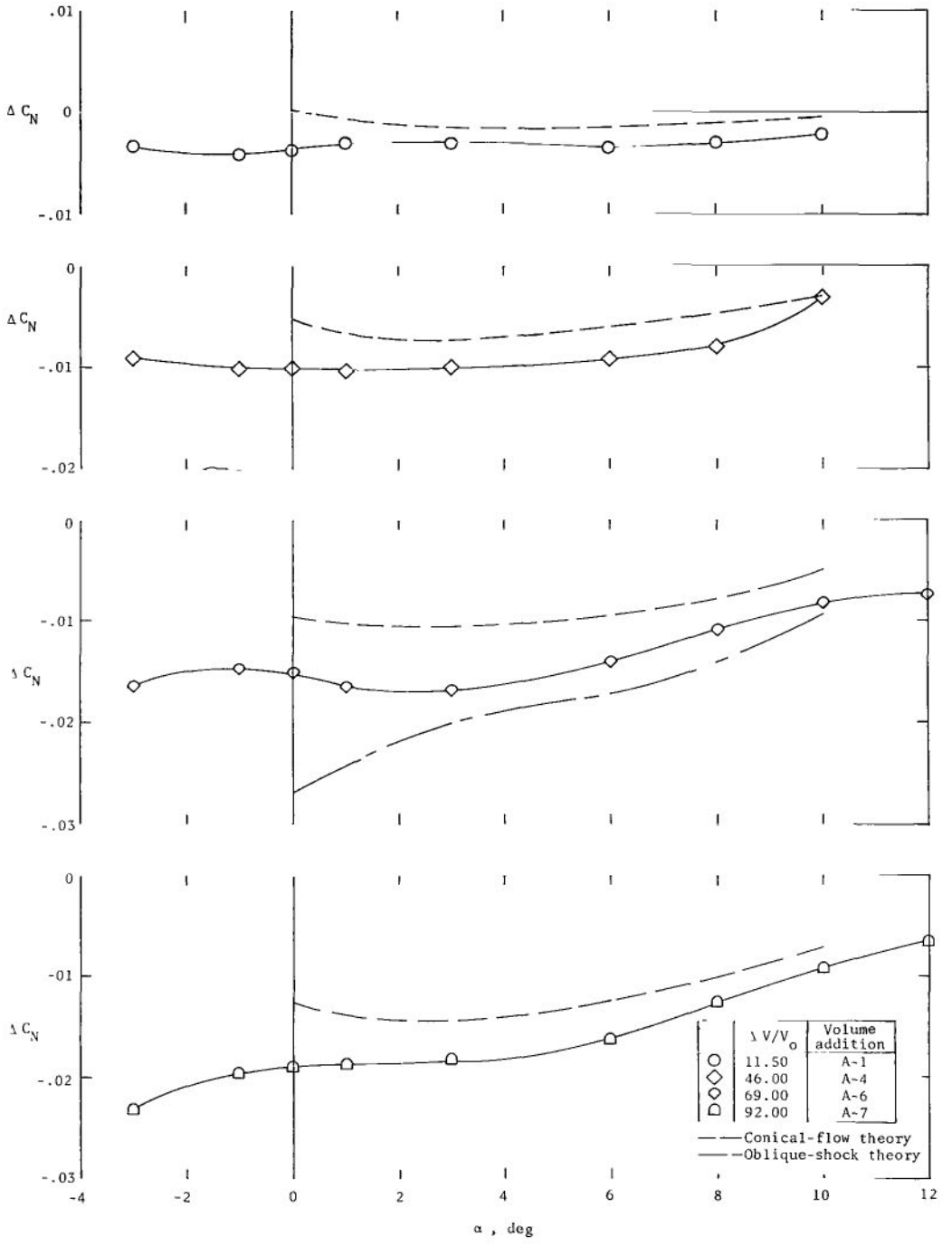

(a) Normal-force increments.

Figure 7.- Increments in normal and axial force for some volume additions of group A.

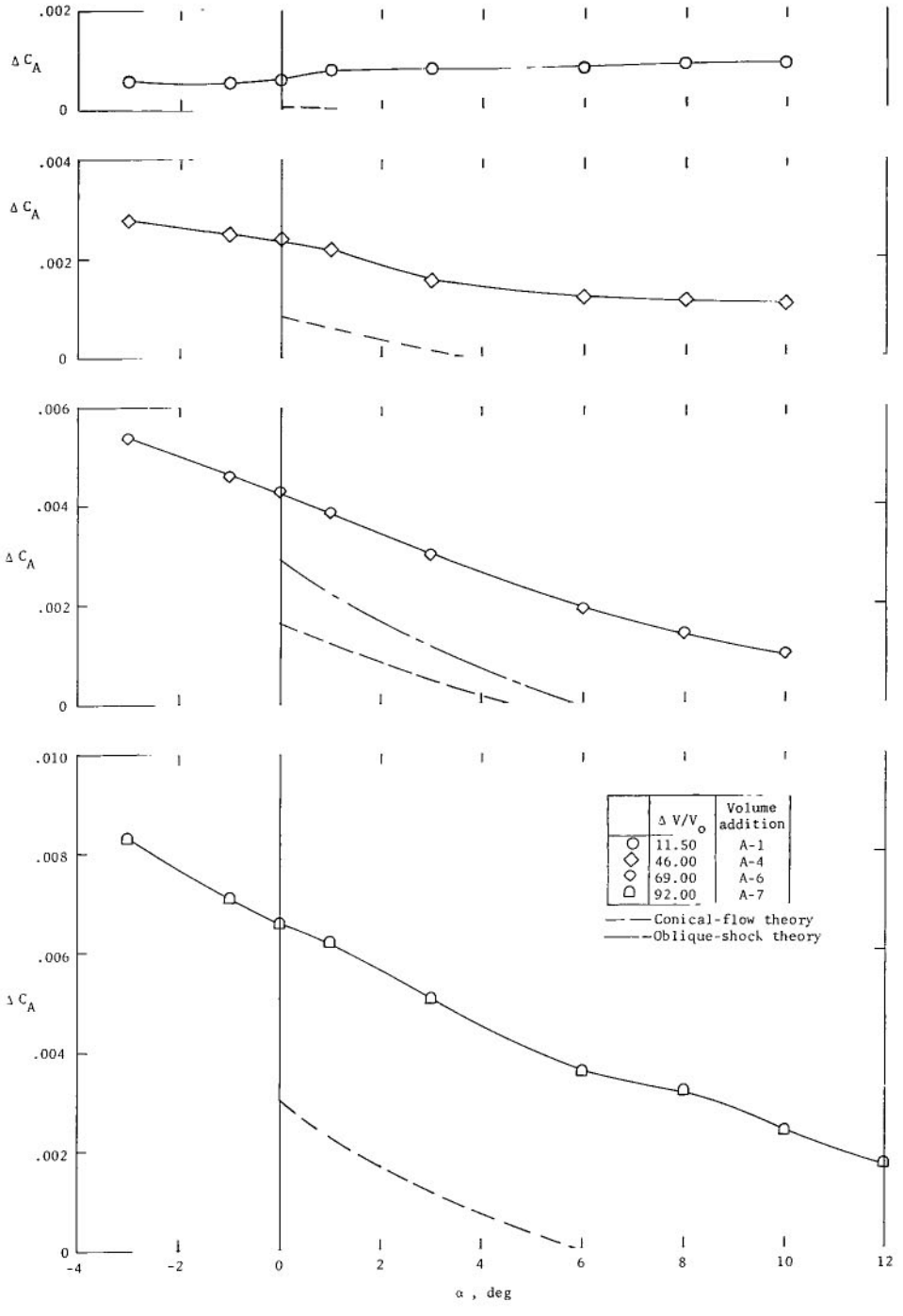

(b) Axial-force increments.

Figure 7.- Concluded.

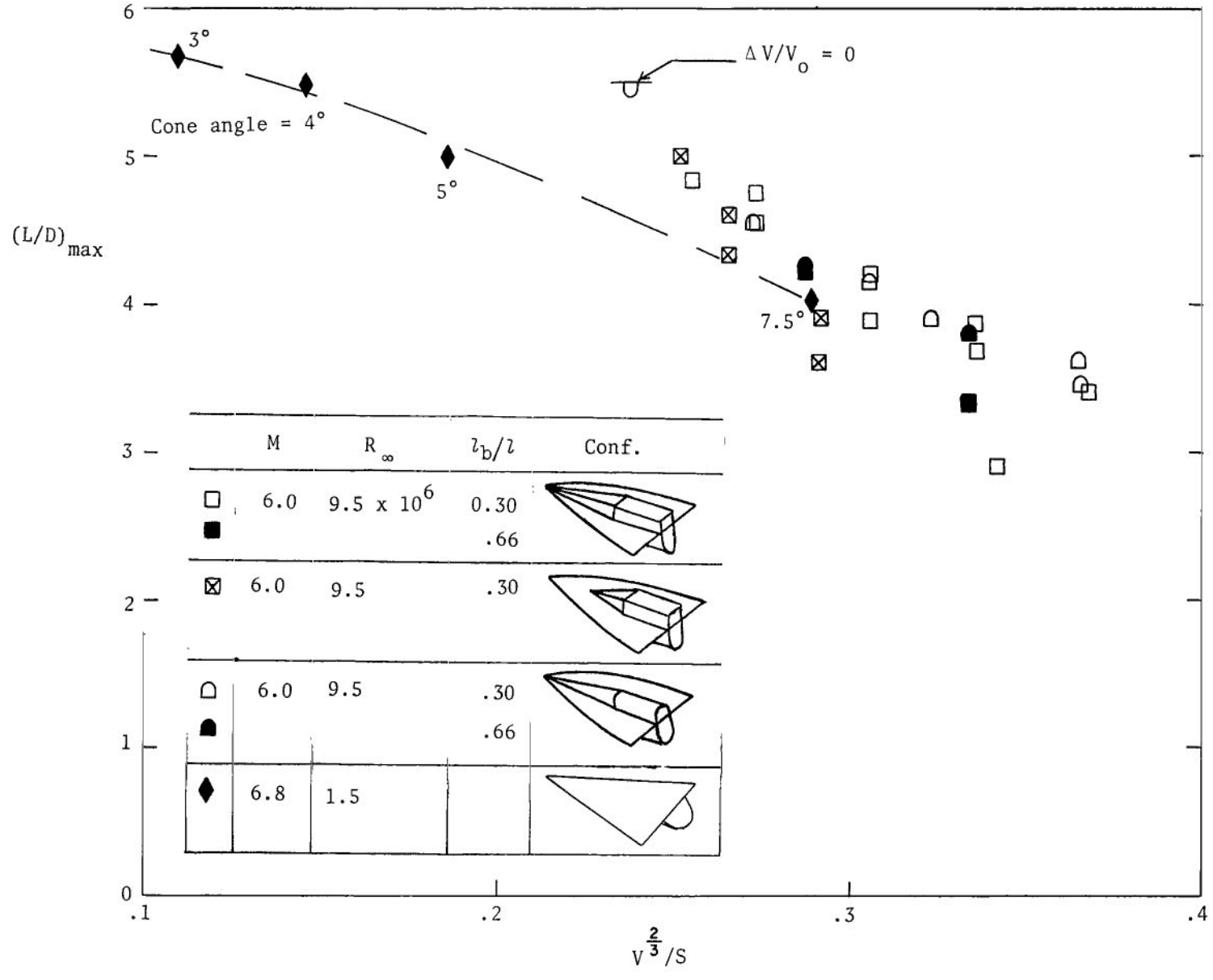

Figure 8.- Variation of $(L/D)_{max}$ with volume parameter.

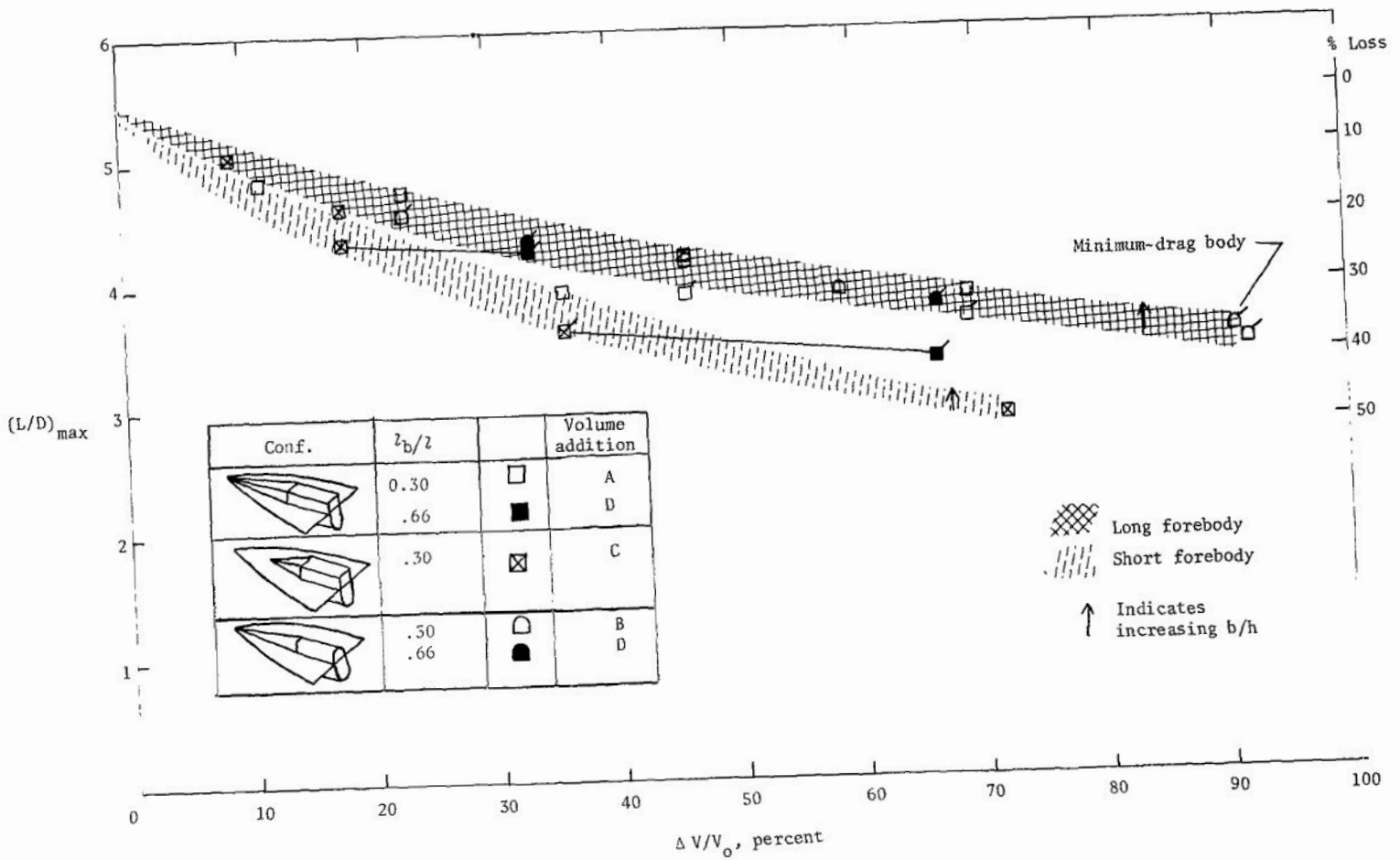

Figure 9.- Variation of $(L/D)_{max}$ with percentage volume added. Flagged symbols indicate forebody slope is greater than α for $(L/D)_{max}$, and solid lines connect volume additions with the same forebody.

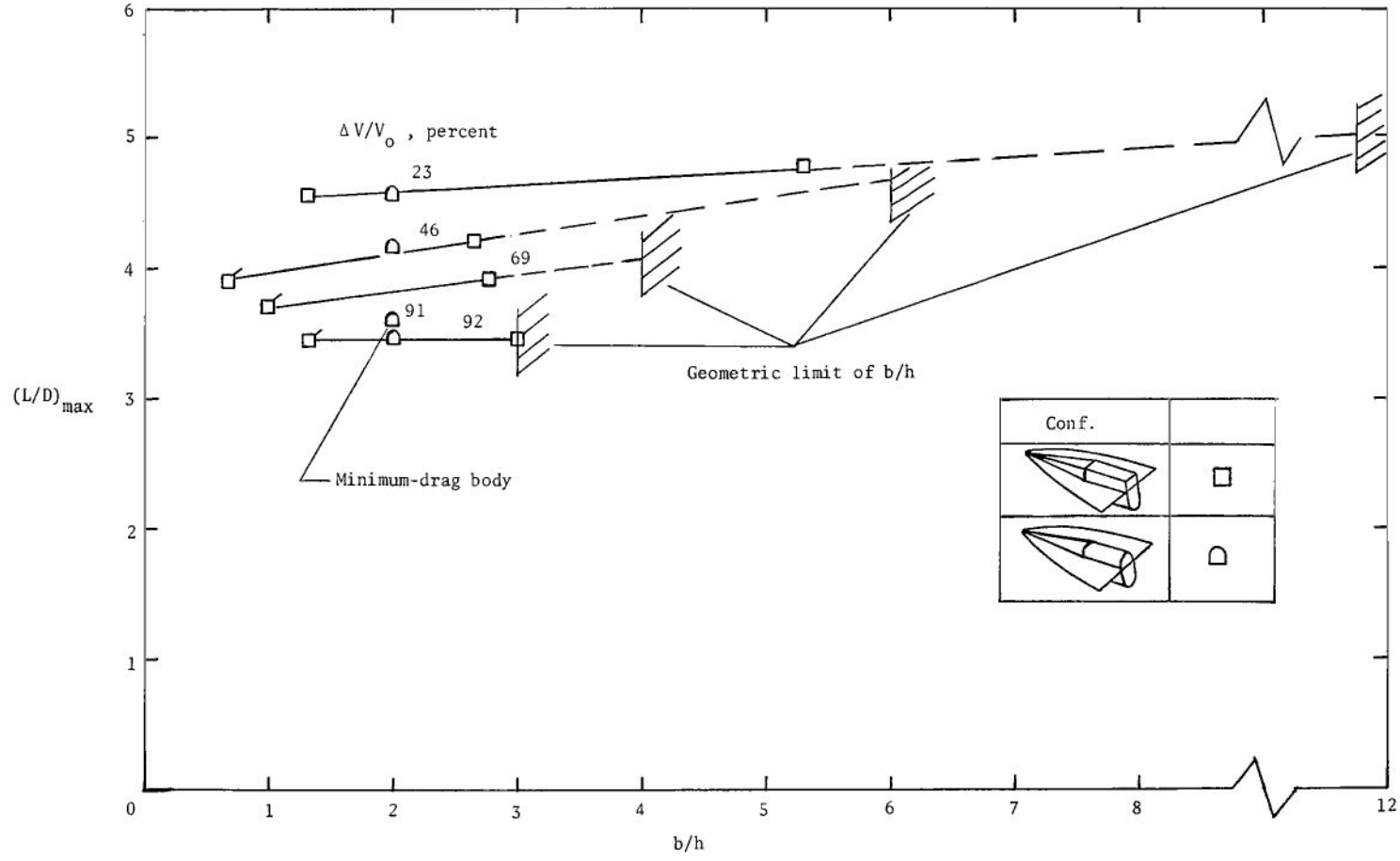

Figure 10.- Effect of b/h on $(L/D)_{max}$ for a given volume. Flagged symbols indicate that the volume addition is exposed to the free-stream flow at α for $(L/D)_{max}$. Geometric limit of b/h is where edge of volume addition coincides with wing leading edge.

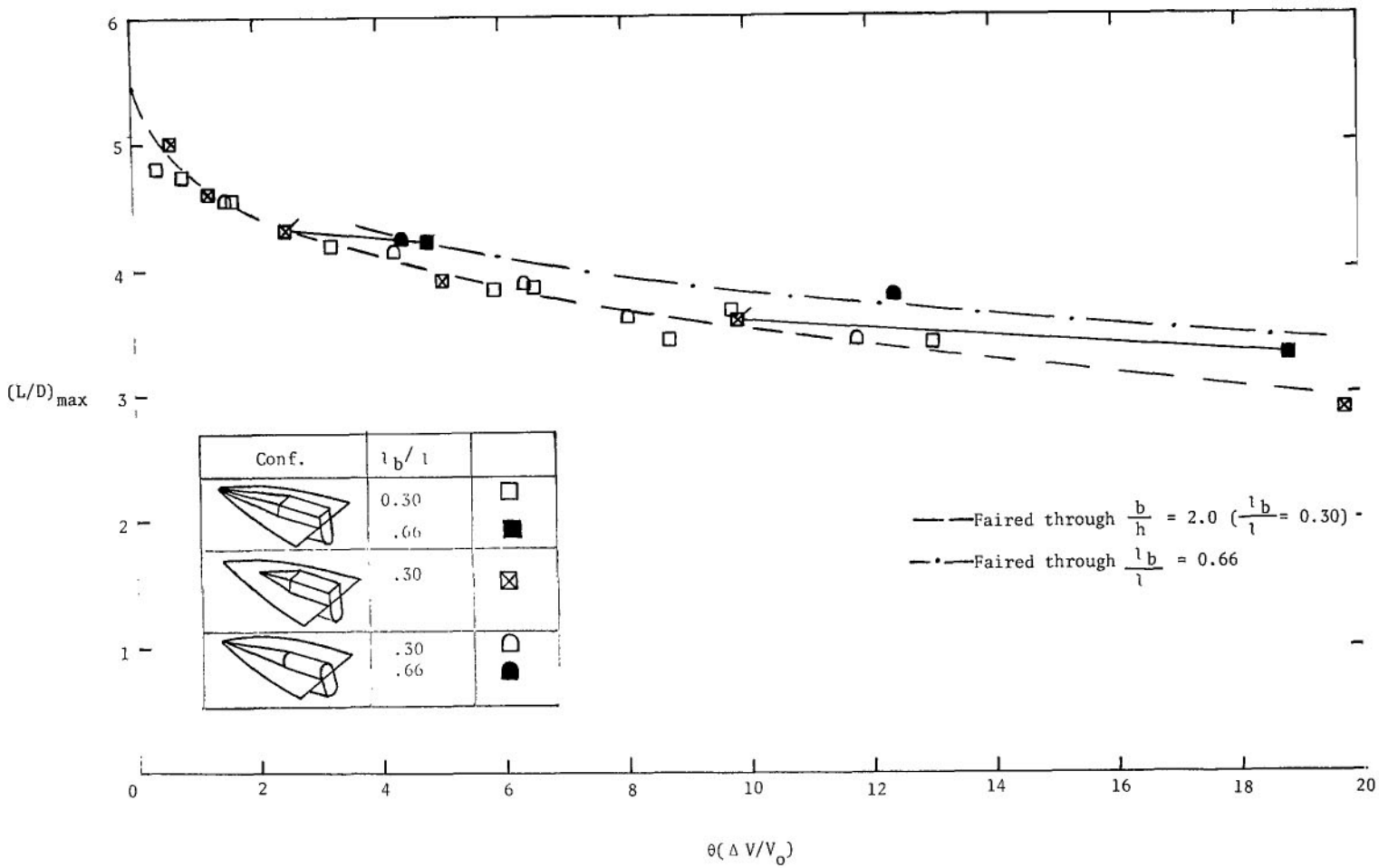

Figure 11.- Correlation of data with forebody-slope volume parameter. Flagged symbols indicate short-forebody volume additions that were moved to the wing apex, and solid lines connect points having the same forebody.

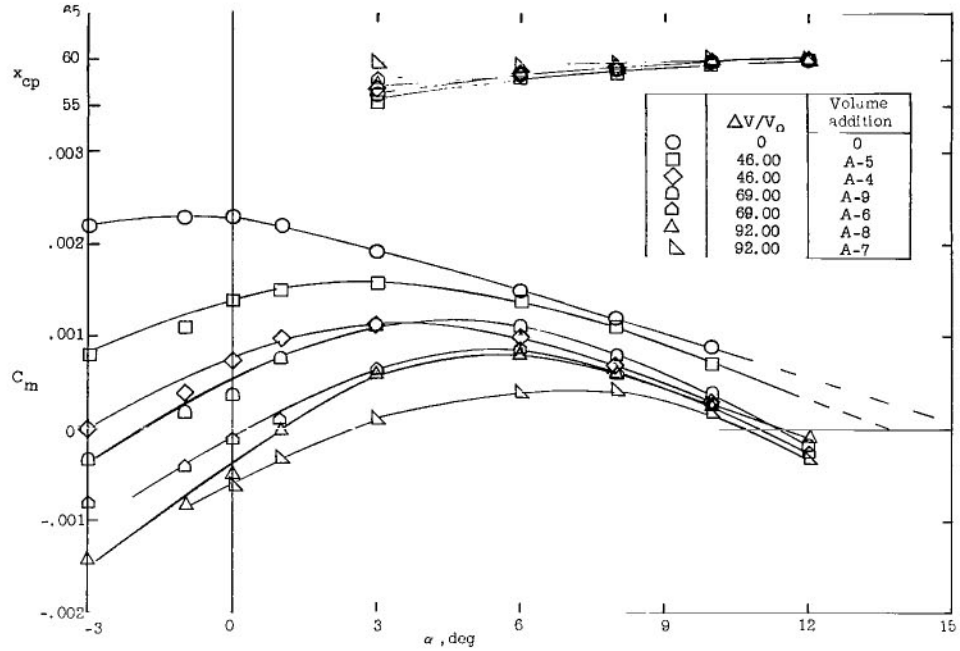

(a) Rectangular cross section.

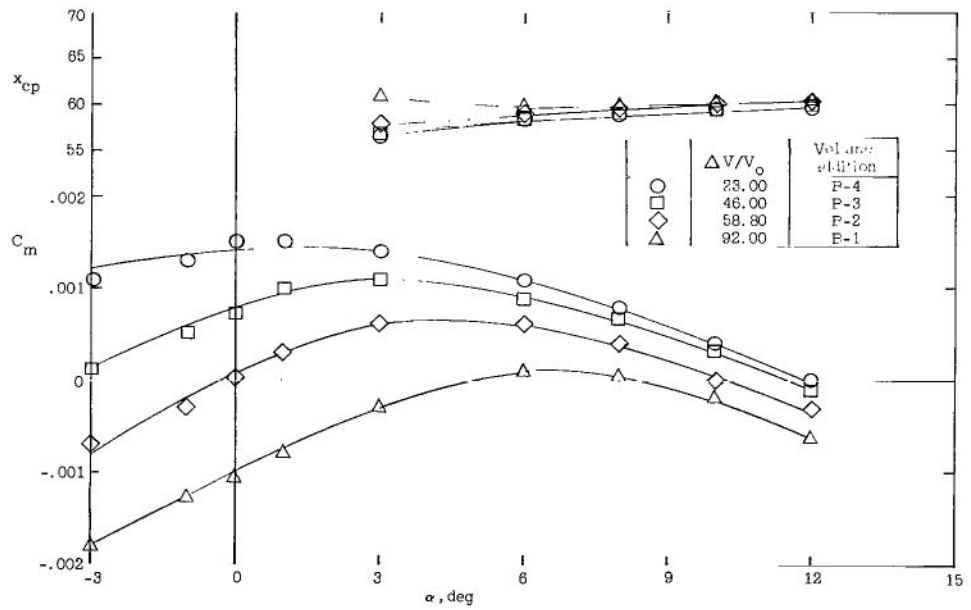

(b) Semicircular section.

Figure 12.- Effect of volume addition on moment coefficient.

"The aeronautical and space activities of the United States shall be conducted so as to contribute . . . to the expansion of human knowledge of phenomena in the atmosphere and space. The Administration shall provide for the widest practicable and appropriate dissemination of information concerning its activities and the results thereof."

—NATIONAL AERONAUTICS AND SPACE ACT OF 1958

NASA SCIENTIFIC AND TECHNICAL PUBLICATIONS

TECHNICAL REPORTS: Scientific and technical information considered important, complete, and a lasting contribution to existing knowledge.

TECHNICAL NOTES: Information less broad in scope but nevertheless of importance as a contribution to existing knowledge.

TECHNICAL MEMORANDUMS: Information receiving limited distribution because of preliminary data, security classification, or other reasons.

CONTRACTOR REPORTS: Scientific and technical information generated under a NASA contract or grant and considered an important contribution to existing knowledge.

TECHNICAL TRANSLATIONS: Information published in a foreign language considered to merit NASA distribution in English.

SPECIAL PUBLICATIONS: Information derived from or of value to NASA activities. Publications include conference proceedings, monographs, data compilations, handbooks, sourcebooks, and special bibliographies.

TECHNOLOGY UTILIZATION PUBLICATIONS: Information on technology used by NASA that may be of particular interest in commercial and other non-aerospace applications. Publications include Tech Briefs, Technology Utilization Reports and Notes, and Technology Surveys.

Details on the availability of these publications may be obtained from:

SCIENTIFIC AND TECHNICAL INFORMATION DIVISION

NATIONAL AERONAUTICS AND SPACE ADMINISTRATION

Washington, D.C. 20546